[redacted]

ORNL-2387, Part 6
C-85 – Reactors – Aircraft Nuclear Propulsion Systems Cy. 125 A

AEC RESEARCH AND DEVELOPMENT REPORT

MARTIN MARIETTA ENERGY SYSTEMS LIBRARIES

3 4456 0251029 0

Jan. 80

DECLASSIFIED
CLASSIFICATION CHANGED TO:
BY AUTHORITY OF:
BY:

AIRCRAFT NUCLEAR PROPULSION PROJECT

QUARTERLY PROGRESS REPORT

FOR PERIOD ENDING SEPTEMBER 30, 1957

CENTRAL RESEARCH LIBRARY
DOCUMENT COLLECTION
LIBRARY LOAN COPY
DO NOT TRANSFER TO ANOTHER PERSON
If you wish someone else to see this document, send in name with document and the library will arrange a loan.

OAK RIDGE NATIONAL LABORATORY • U.S. ATOMIC ENERGY COMMISSION

[redacted]

OAK RIDGE NATIONAL LABORATORY
OPERATED BY
UNION CARBIDE NUCLEAR COMPANY
Division of Union Carbide Corporation
UCC
POST OFFICE BOX X · OAK RIDGE, TENNESSEE

[redacted]

LEGAL NOTICE

This report was prepared as an account of Government sponsored work. Neither the United States, nor the Commission, nor any person acting on behalf of the Commission:

A. Makes any warranty or representation, express or implied, with respect to the accuracy, completeness, or usefulness of the information contained in this report, or that the use of any information, apparatus, method, or process disclosed in this report may not infringe privately owned rights; or

B. Assumes any liabilities with respect to the use of, or for damages resulting from the use of any information, apparatus, method, or process disclosed in this report.

As used in the above, "person acting on behalf of the Commission" includes any employee or contractor of the Commission to the extent that such employee or contractor prepares, handles or distributes, or provides access to, any information pursuant to his employment or contract with the Commission.

[redacted]

ORNL-2387, Part 6
C-85 – Reactors – Aircraft Nuclear Propulsion Systems

This document consists of 30 pages.

Copy 25 of 254 copies. Series A.

Contract No. W-7405-eng-26

AIRCRAFT NUCLEAR PROPULSION PROJECT

QUARTERLY PROGRESS REPORT

For Period Ending September 30, 1957

W. H. Jordan, Director
S. J. Cromer, Co-Director
A. J. Miller, Assistant Director

DATE ISSUED

FEB 7 1958

OAK RIDGE NATIONAL LABORATORY
Operated by
UNION CARBIDE NUCLEAR COMPANY
Division of Union Carbide Corporation
Post Office Box X
Oak Ridge, Tennessee

[redacted]

MARTIN MARIETTA ENERGY SYSTEMS LIBRARIES
3 4456 0251029 0

[redacted]

[redacted]

[redacted]

INTERNAL DISTRIBUTION

1. R. G. Affel
2. C. J. Barton
3. M. Bender
4. D. S. Billington
5. F. F. Blankenship
6. E. P. Blizard
7. C. J. Borkowski
8. W. F. Boudreau
9. G. E. Boyd
10. M. A. Bredig
11. E. J. Breeding
12. W. E. Browning
13. F. R. Bruce
14. A. D. Callihan
15. D. W. Cardwell
16. C. E. Center (K-25)
17. R. A. Charpie
18. R. L. Clark
19. C. E. Clifford
20. J. H. Coobs
21. W. B. Cottrell
22. R. S. Crouse
23. F. L. Culler
24. D. R. Cuneo
25. J. H. DeVan
26. L. M. Doney
27. D. A. Douglas
28. W. K. Eister
29. L. B. Emlet (K-25)
30. D. E. Ferguson
31. A. P. Fraas
32. J. H. Frye
33. W. T. Furgerson
34. R. J. Gray
35. A. T. Gresky
36. W. R. Grimes
37. A. G. Grindell
38. E. Guth
39. C. S. Harrill
40. M. R. Hill
41. E. E. Hoffman
42. H. W. Hoffman
43. A. Hollaender
44. A. S. Householder
45. J. T. Howe
46. W. H. Jordan
47. G. W. Keilholtz
48. C. P. Keim
49. F. L. Keller
50. M. T. Kelley
51. F. Kertesz
52. J. J. Keyes
53–54. J. A. Lane
55. R. B. Lindauer
56. R. S. Livingston
57. R. N. Lyon
58. H. G. MacPherson
59. R. E. MacPherson
60. F. C. Maienschein
61. W. D. Manly
62. E. R. Mann
63. L. A. Mann
64. W. B. McDonald
65. J. R. McNally
66. F. R. McQuilkin
67. R. V. Meghreblian
68. R. P. Milford
69. A. J. Miller
70. R. E. Moore
71. J. G. Morgan
72. K. Z. Morgan
73. E. J. Murphy
74. J. P. Murray (Y-12)
75. M. L. Nelson
76. G. J. Nessle
77. R. B. Oliver
78. L. G. Overholser
79. P. Patriarca
80. S. K. Penny
81. A. M. Perry
82. D. Phillips
83. J. C. Pigg
84. P. M. Reyling
85. A. E. Richt
86. M. T. Robinson
87. H. W. Savage
88. A. W. Savolainen
89. R. D. Schultheiss
90. D. Scott
91. J. L. Scott

[redacted]

[redacted]

92. E. D. Shipley
93. A. Simon
94. O. Sisman
95. J. Sites
96. M. J. Skinner
97. A. H. Snell
98. C. D. Susano
99. J. A. Swartout
100. E. H. Taylor
101. R. E. Thoma
102. D. B. Trauger
103. D. K. Trubey
104. G. M. Watson
105. A. M. Weinberg
106. J. C. White
107. G. D. Whitman
108. E. P. Wigner (consultant)
109. G. C. Williams
110. J. C. Wilson
111. C. E. Winters
112. W. Zobel
113–115. ORNL – Y-12 Technical Library, Document Reference Section
116–122. Laboratory Records Department
123. Laboratory Records, ORNL R.C.
124–126. Central Research Library

EXTERNAL DISTRIBUTION

127–129. Air Force Ballistic Missile Division
130–131. AFPR, Boeing, Seattle
132. AFPR, Boeing, Wichita
133. AFPR, Curtiss-Wright, Clifton
134. AFPR, Douglas, Long Beach
135–137. AFPR, Douglas, Santa Monica
138. AFPR, Lockheed, Burbank
139–140. AFPR, Lockheed, Marietta
141. AFPR, North American, Canoga Park
142. AFPR, North American, Downey
143. Air Force Special Weapons Center
144. Air Research and Development Command (RDGN)
145. Air Research and Development Command (RDTAPS)
146–159. Air Research and Development Command (RDZPSP)
160. Air Technical Intelligence Center
161. Air University Library
162–164. ANP Project Office, Convair, Fort Worth
165. Argonne National Laboratory
166. Armed Forces Special Weapons Project, Sandia
167. Armed Forces Special Weapons Project, Washington
168. Assistant Secretary of the Air Force, R&D
169–174. Atomic Energy Commission, Washington
175. Bettis Plant (WAPD)
176. Bureau of Aeronautics
177. Bureau of Aeronautics General Representative
178. BAR, Aerojet-General, Azusa
179. BAR, Convair, San Diego
180. BAR, Glenn L. Martin, Baltimore
181. BAR, Goodyear Aircraft, Akron
182. BAR, Grumman Aircraft, Bethpage
183. Bureau of Ships
184. Bureau of Yards and Docks
185. Chicago Operations Office
186. Chicago Patent Group
187. Curtiss-Wright Corporation

[redacted]

[redacted]

188–191. General Electric Company (ANPD)
192. Hartford Area Office
193. Idaho Operations Office
194. Knolls Atomic Power Laboratory
195. Lockland Area Office
196. Los Alamos Scientific Laboratory
197. Martin-Marietta Aircraft Company
198. National Advisory Committee for Aeronautics, Cleveland
199. National Advisory Committee for Aeronautics, Washington
200. Naval Air Development Center
201. Naval Air Material Center
202. Naval Air Turbine Test Station
203. Naval Research Laboratory
204. Nuclear Development Corporation of America
205. Office of Naval Research
206. Office of the Chief of Naval Operations (OP-361)
207. Patent Branch, Washington
208–211. Pratt and Whitney Aircraft Division
212. San Francisco Operations Office
213. Sandia Corporation
214. Sandia Corporation, Livermore
215. School of Aviation Medicine
216. USAF Headquarters
217. USAF Project RAND
218. U. S. Naval Radiological Defense Laboratory
219–220. University of California Radiation Laboratory, Livermore
221–238. Wright Air Development Center (WCOSI-3)
239–253. Technical Information Service Extension, Oak Ridge
254. Division of Research and Development, AEC, ORO

[redacted]

[redacted]

FOREWORD

This portion, Part 6. Aircraft Shielding, of the Aircraft Nuclear Propulsion Project Quarterly Progress Report falls in AEC category C-85, Reactors – Aircraft Nuclear Propulsion Systems, and is therefore being issued separately in order not to further limit distribution of the material that falls in AEC category C-84, Reactors – Special Features of Aircraft Reactors, which has been issued as ORNL-2387, Parts 1–5.

[redacted]

[redacted]

[redacted]

[redacted]

CONTENTS

PART 6. AIRCRAFT SHIELDING

6.1. TOWER SHIELDING FACILITY 3

Summary 3

Penetration of Air-Scattered Fast Neutrons from the TSF Reactor Through the Sides of a Cylindrical Crew Compartment 3

Determination of the Direct-Beam Integral 4

Experimental Configurations 6

Measurements in Air and in the Crew Compartment 7

Determination of the Air-Scattering Probabilities 11

Relaxation Lengths in the Water in the Crew-Compartment Side Shield 17

[redacted]

Part 6

AIRCRAFT SHIELDING

E. P. Blizard

6.1. TOWER SHIELDING FACILITY

C. E. Clifford

SUMMARY

Measurements of the penetration of broad-beam air-scattered fast neutrons through the sides of a cylindrical crew-compartment mockup were completed. The mockup consisted of a 36-in.-dia cylindrical cavity surrounded by 0, 2, 4, 6, or 8 in. of water or oil side shielding. It was suspended in air at a height of 190 ft and a horizontal distance of 64 ft from the TSF reactor. Shielding at the rear (nearest to reactor) of the mockup reduced the contribution of the direct-beam radiation at the center of the cavity to less than 1% of the lowest measured dose rate. As a result of these measurements more reliable air-scattering probabilities are now available for predictions of the neutron dose which will penetrate the sides of a crew compartment. Since the probabilities previously determined were largely based on measurements in the TSF detector tank, earlier calculations required an integration involving the factors $l^2P^s(\theta)$ (the probability of neutrons leaving the reactor at a horizontal beam angle θ and scattering in air to the surface of a crew compartment),

$$e^{-\int_0^{T_s} dt/\lambda_s^s}$$

(the attenuation term for the given side shield thickness), and f_s^s (a factor accounting for the focusing of the neutrons in the center of the cylindrical cavity). The air-scattering probabilities, $2\pi l^2 P^s_{s,c}(\theta, T_s)$, determined on the basis of these latest measurements are equal to the products of the three factors and are defined as $2\pi l^2$ times the measured dose rates at the center of the crew compartment divided by the total direct-beam dose rate from the reactor. Therefore the definition of the focusing factor f_s^s is the ratio

$$\frac{2\pi l^2 P^s_{s,c}(\theta, T_s)}{l^2 P^s(\theta)\, e^{-\int_0^{T_s} dt/\lambda_s^s}} .$$

Values of this ratio were determined and, contrary to the previous indications, f_s^s was found to be dependent on θ.

Instantaneous relaxation lengths for consecutive 2-in. increments of the side shielding water thickness were obtained for ρ = 20 and 40 cm. By using the assumption that λ_s^s varies with ρ as λ_d varies with ρ (λ_d = the direct-beam relaxation length in the reactor tank), relaxation lengths for ρ = 45 cm were calculated and compared with similar data obtained from detector tank measurements. The results agreed to within 15%.

No formal analysis of the data obtained with oil side shielding was attempted, since the shapes of the dose rate vs θ curves for oil and water were similar to within experimental error. The dose rates with oil side shielding were slightly lower than those with water side shielding.

An attempt was also made to determine the relative effectiveness of the position of the side shielding thickness from the rear to the front of the crew-compartment mockup. The data obtained were converted to percentage dose rates for each individual tank, and the dose rates were divided by the total solid angle subtended by the tank at the detector in order to determine the average percentage dose rate per unit solid angle. The results are presented in terms of the average angle of the entering radiation at the detector.

PENETRATION OF AIR-SCATTERED FAST NEUTRONS FROM THE TSF REACTOR THROUGH THE SIDES OF A CYLINDRICAL CREW COMPARTMENT

V. R. Cain — F. N. Greene[1]
C. R. Fink[1] — W. E. Price[2]

Fast neutrons that scatter in air and then penetrate the sides of a crew shield will constitute a significant fraction of the total dose in the crew compartment of an aircraft having a divided shield. In an attempt to determine the variation of this contribution with the amount of shielding on the side of the crew compartment, an experiment was performed in which fast-neutron dose rates were measured at the center of a cylindrical crew

[1]On assignment from The Glenn L. Martin Co.

[2]On assignment from Pratt & Whitney Aircraft.

compartment for side shielding thicknesses that were varied from 0 to 8 in. in 2-in. increments. Both water and a light transformer oil were used as the shielding materials. A shadow shield on the rear of the crew compartment limited the contribution of the direct beam to the measurement at the center of the crew compartment to less than 1% of the lowest measured dose rate. The measurements were taken both as a function of thickness of the water shield at the reactor, which was separated from the crew compartment by a constant horizontal distance, and as a function of the horizontal angle at which the neutron beam was emitted from the reactor tank.

The results of the experiment were used to determine the probabilities of scattering into the crew compartment, and the probabilities were compared with those previously obtained[3] on the basis of measurements made in the TSF detector tank. The probabilities determined from the crew-compartment measurements are considered to be the more reliable ones, because the geometry of the experiment more nearly mocked up an actual reactor–crew shield configuration.

Determination of the Direct-Beam Integral

An accurate determination of the direct-beam integral, that is, the total direct-beam dose rate leaving the surface of the TSF reactor tank, was necessary in order to obtain reliable air-scattering probabilities. In the past, direct-beam dose rates were obtained by subtracting the *estimated* air-scattered dose rates from measured total dose rates. These *estimated* air-scattered dose rates were obtained by extrapolating the total dose rates measured at large values of the angle θ back to low values of θ and assuming that this extrapolation represented the air-scattered dose rate. (The angle θ is the horizontal angle between the center line of the beam and an axis through the centers of the reactor tank and the dosimeter.) These estimated dose rates were then subtracted from the total measured dose rates at low values of θ to obtain the direct-beam integral. Since even a small inaccuracy in the magnitude of the direct-beam dose rate at small angles of θ could cause an appreciable error in the calculation of the direct-beam integral, it was felt that a more accurate and more direct determination of the direct-beam integral should be made. Therefore, an experiment was performed to measure this quantity directly.

The direct beam leaving the reactor tank was mapped as a function of θ for reactor water shield thicknesses (ρ) of 20 and 40 cm. The configuration used for this mapping is shown in Fig. 6.1.1. A triple-barreled Hurst-type fast-neutron dosimeter, which was shielded on all sides except on the side toward the reactor, was placed 61.5 ft from the center of the reactor tank. A 3-ft-dia collimator (two cylinders separated by a 15-in.-thick water-filled annulus) was positioned between the reactor

[3]M. F. Valerino, *ANP Quar. Prog. Rep. June 10, 1955*, ORNL-1896, p 206.

UNCLASSIFIED
2-01-056-20-D-577

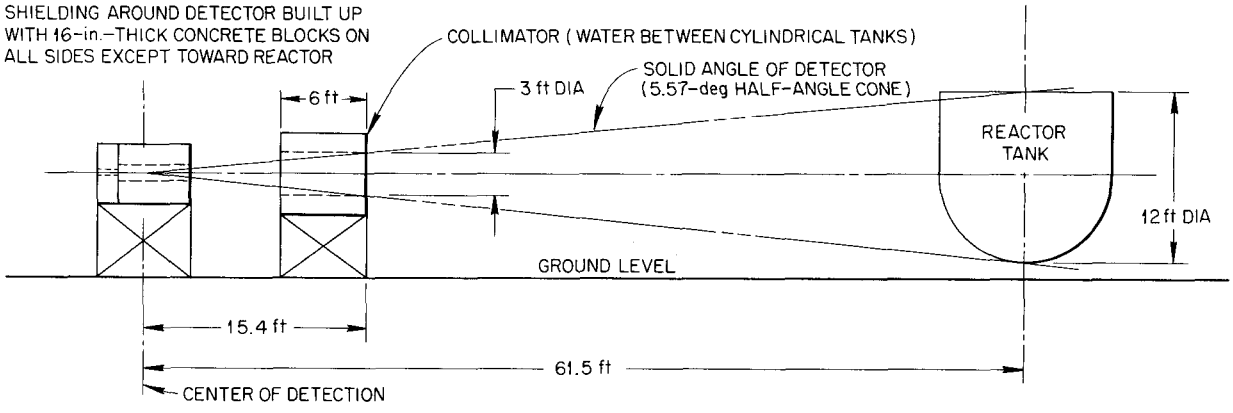

Fig. 6.1.1. Geometry Used in Experiment To Measure the Fast-Neutron Direct-Beam Dose Rate from the TSF Reactor.

tank and the dosimeter so that the solid angle seen through the collimator from the dosimeter center of detection just included the reactor tank, which was suspended in air slightly above the pool. Fast-neutron dose-rate measurements as a function of the horizontal reactor angle θ were made both with the collimator open and with it plugged with sufficient amounts of water and concrete to bring the dose rate coming through the collimator to well below background. The results of all the measurements are given in Table 6.1.1, and the differences between these foreground and

Table 6.1.1. Separation of the Total Fast-Neutron Dose Rate in Air into the Direct-Beam and Air-Scattered Components

θ (deg)	Fast-Neutron Dose Rate (ergs/g·hr·w)						
	Foreground* (A)	Background* (B)	Direct-Beam ($C = A - B$)	Total in Air (D)	Air-Scattered ($D - C$)	Corrected Air-Scattered (E)	Corrected Direct-Beam ($D - E$)
				ρ = 20 cm			
0	2.32×10^{-2}	3.74×10^{-4}	2.28×10^{-2}	2.48×10^{-2}	2.0×10^{-3}	5.37×10^{-3}	1.94×10^{-2}
15	1.91×10^{-2}	3.26×10^{-4}	1.88×10^{-2}	2.15×10^{-2}	2.7×10^{-3}	4.86×10^{-3}	1.66×10^{-2}
30	1.32×10^{-2}	2.69×10^{-4}	1.29×10^{-2}	1.55×10^{-2}	2.6×10^{-3}	3.44×10^{-3}	1.20×10^{-2}
45	7.79×10^{-3}	1.92×10^{-4}	7.60×10^{-3}	0.947×10^{-2}	1.87×10^{-3}	2.37×10^{-3}	0.710×10^{-2}
60	2.79×10^{-3}	1.14×10^{-4}	2.68×10^{-3}	0.404×10^{-2}	1.36×10^{-3}	1.36×10^{-3}	0.268×10^{-2}
75	7.86×10^{-4}	7.02×10^{-5}	7.16×10^{-4}	0.160×10^{-2}	0.88×10^{-3}	0.88×10^{-3}	0.072×10^{-2}
90	1.18×10^{-4}	4.64×10^{-5}	7.20×10^{-5}	0.062×10^{-2}	0.55×10^{-3}	0.55×10^{-3}	0.007×10^{-2}
120				0.037×10^{-2}	0.37×10^{-3}	0.37×10^{-3}	
150				0.031×10^{-2}	0.31×10^{-3}	0.31×10^{-3}	
180				0.027×10^{-2}	0.27×10^{-3}	0.27×10^{-3}	
				ρ = 40 cm			
0	1.67×10^{-3}	2.82×10^{-5}	1.64×10^{-3}	1.75×10^{-3}	1.1×10^{-4}	3.25×10^{-4}	1.43×10^{-3}
15	1.42×10^{-3}	2.48×10^{-5}	1.40×10^{-3}	1.53×10^{-3}	1.3×10^{-4}	2.86×10^{-4}	1.24×10^{-3}
30	9.29×10^{-4}	1.86×10^{-5}	9.10×10^{-4}	1.03×10^{-3}	1.2×10^{-4}	1.99×10^{-4}	0.83×10^{-3}
45	5.34×10^{-4}	1.34×10^{-5}	5.21×10^{-4}	0.625×10^{-3}	1.04×10^{-4}	1.44×10^{-4}	0.48×10^{-3}
60	2.08×10^{-4}	7.81×10^{-6}	2.00×10^{-4}	0.280×10^{-3}	0.80×10^{-4}	0.80×10^{-4}	0.20×10^{-3}
75	6.63×10^{-5}	4.72×10^{-6}	6.16×10^{-5}	0.108×10^{-3}	0.46×10^{-4}	0.46×10^{-4}	0.062×10^{-3}
90	1.32×10^{-5}	2.95×10^{-6}	1.02×10^{-5}	0.041×10^{-3}	0.31×10^{-4}	0.31×10^{-4}	0.010×10^{-3}
120				0.022×10^{-3}	0.22×10^{-4}	0.22×10^{-4}	
150				0.019×10^{-3}	0.19×10^{-4}	0.19×10^{-4}	
180				0.016×10^{-3}	0.16×10^{-4}	0.16×10^{-4}	

*Measurements taken with geometry shown in Fig. 6.1.1.

background measurements, also given in Table 6.1.1, represent the measured direct-beam dose rates, which are plotted in Fig. 6.1.2.

When the measured direct-beam dose rate was subtracted from the total dose rate measured at a height of 190 ft, the shape of the resulting air-scattered dose-rate curve (see Fig. 6.1.2) appeared to be unrealistic for $\theta = 0$ to 60 deg and, in particular, for $\theta = 0$ to 30 deg. The unexpected shape is probably due to low-angle air scattering into the collimator and possibly some collimator scattering. Since the dose rates later measured in the crew compartment at a height of 190 ft (discussed below) can be assumed to result only from air-scattered neutrons, the slopes of the crew-compartment dose-rate curves should be good approximations of the slopes of the curves representing the air-scattered dose rates in air for $\theta < 90$ deg. The curve representing the measurements in the crew compartment with no side shielding was therefore normalized to the air-scattering curve between $\theta = 60$ deg and $\theta = 90$ deg, and the normalized curve was assumed to give the correct air-scattered dose rates from $\theta = 0$ to 60 deg. The corrected dose rates were then subtracted from the total measured dose rates to obtain the corrected direct-beam dose rates, $D_d(\theta)$. These results are also plotted in Fig. 6.1.2 and listed in Table 6.1.1. An integration of $D_d(\theta)$ was performed over all angles to obtain the total dose rate leaving the surface of the reactor tank:

$$D_{tot} = 2\pi l^2 \int_0^{\pi} D_d(\theta) \sin\theta \, d\theta \, .$$

The values of D_{tot} are 3.04×10^{-2} erg/g·hr·w for $\rho = 20$ cm and 2.18×10^{-3} erg/g·hr·w for $\rho = 40$ cm.

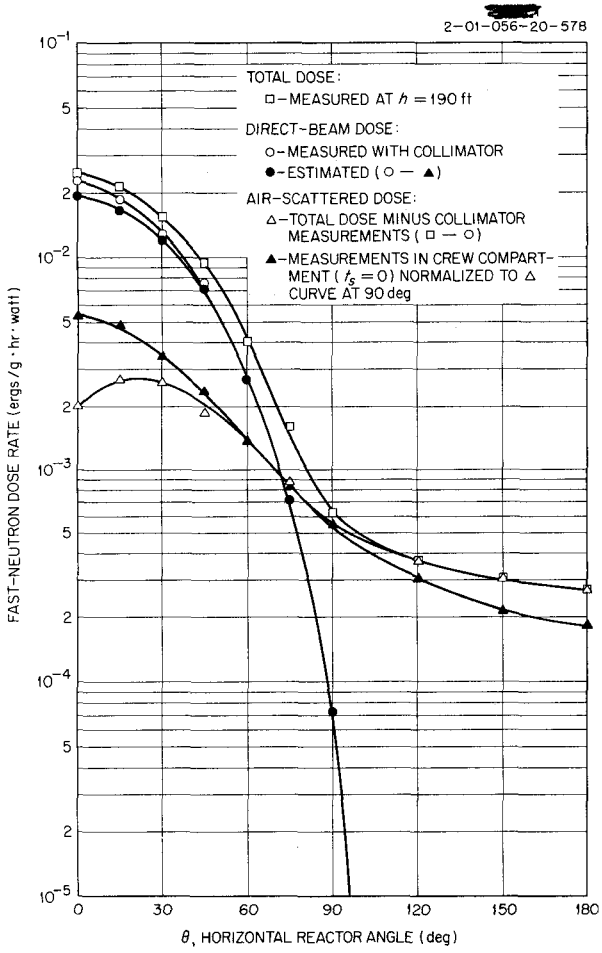

Fig. 6.1.2. Separation of the Total Fast-Neutron Dose Rate in Air into the Direct-Beam and Air-Scattered Components.

Experimental Configurations

The geometry for the measurements in air and in the crew compartment is shown in Fig. 6.1.3.

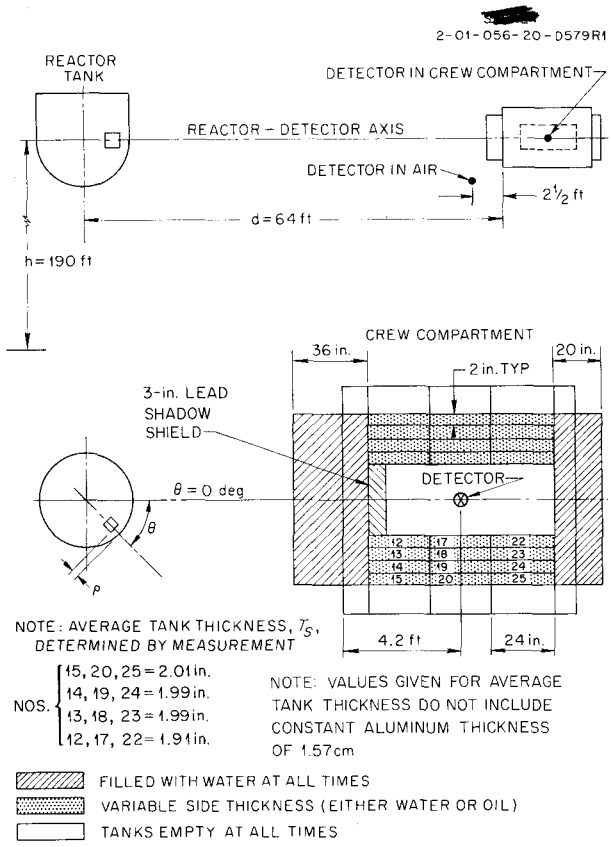

Fig. 6.1.3. Crew-Compartment Configuration.

For all the measurements the reactor was located in the TSF reactor tank and the detector was located on an axis which passed through the center of the reactor tank. At $\theta = 0$ deg, the beam from the reactor was directed at the detector.

The crew compartment used in the experiment consists of a total of 33 compartments which can be filled with a liquid and drained by remote control. It has 12 cylindrical side tanks, arranged in four 2-in.-thick layers, which were used to vary the shielding thickness around a 36-in.-dia cylindrical cavity from 0 to 8 in. in 2-in. increments. Both oil and water were used as the shielding materials. A rear (nearest to reactor) shadow shield (36 in. of water and 3 in. of lead) and a front shadow shield (20 in. of water) remained constant throughout the experiment. This configuration was used because it limited the direct-beam dose rate in the crew compartment to less than 1% of the lowest measured dose rate. In addition to the 12 side compartments used throughout the experiment, there were five 12-in.-thick outermost tanks which were filled with water for one measurement in order to determine whether the background from the radiation entering the front and rear was significant.

All the measurements were made at a height (h) of 190 ft. The distance (d) between the center of the reactor tank and the rear of the crew compartment was 64 ft. For the in-air measurements the distance between the center of the reactor tank and the detector was 61.5 ft.

A determination of the actual thickness of the individual side tanks in the Boeing crew compartment was required because the manufacturing tolerances allowed a 7% error in the nominal 2-in. thickness. The method used consisted of weighing the water content of each side tank. Since manufacturing tolerances for the length and mean circumference of the side tanks could each give maximum errors of 0.5%, the nominal lengths and mean circumferences were used and the thicknesses were solved for. Although there was some variation in the actual thicknesses of the tanks, an average thickness was used for each layer of three tanks. This average thickness was determined on the basis of the actual thicknesses of the rear and middle tanks only, since it was thought, and later confirmed by the experiment, that the dose rate arriving through the front tanks was relatively unimportant.

Measurements in Air and in the Crew Compartment

The fast-neutron dose rates measured at the center of the crew compartment as a function of θ for various thicknesses (T_s) of a water side shield are shown in Figs. 6.1.4 and 6.1.5 for ρ = 20 and 40 cm, respectively, and also in Table 6.1.2. Measurements made in air are also presented in the figures. Only the air-scattered curve has been modified; all other plots represent actual measurements. In line with the current effort to obtain reproducible data,[4] the effect of each variable in the experiment was monitored with a single-barreled Hurst-type dosimeter mounted

[4]F. N. Greene and V. R. Cain, *ANP Quar. Prog. Rep. June 30, 1957*, ORNL-2340 (Part 6), p 19.

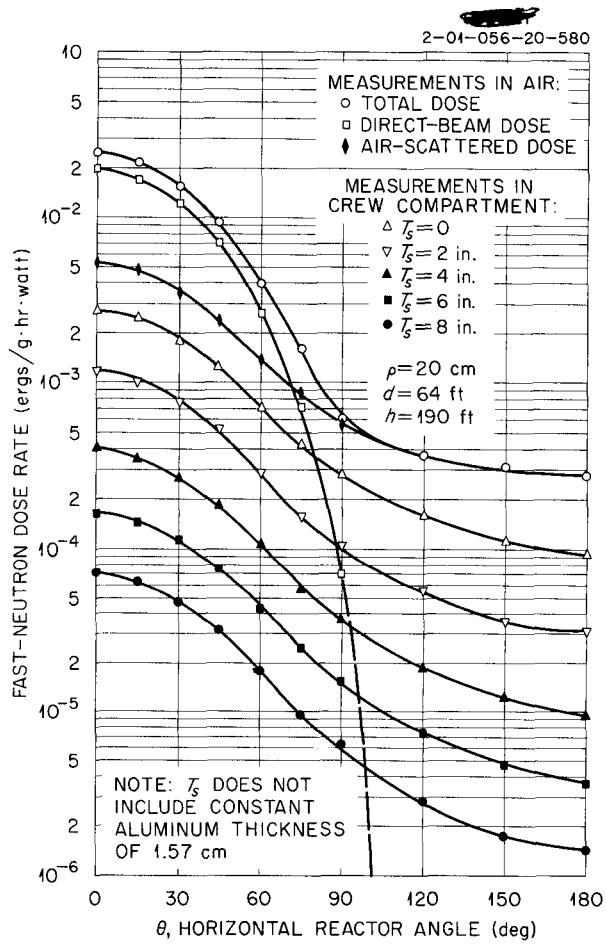

Fig. 6.1.4. Fast-Neutron Dose Rates in Air and in the Crew Compartment (Water Side Shield) as a Function of θ(ρ = 20 cm).

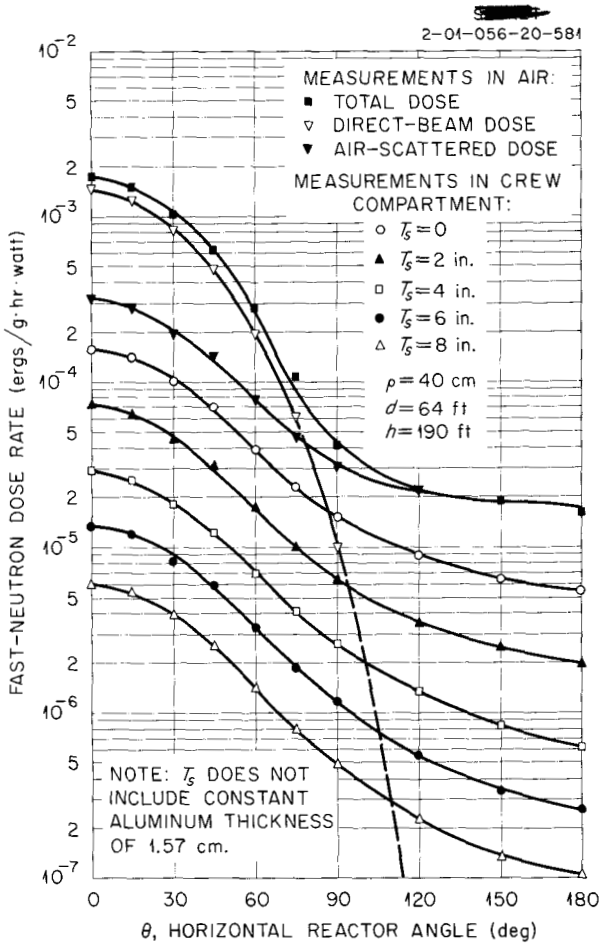

Fig. 6.1.5. Fast-Neutron Dose Rates in Air and in the Crew Compartment (Water Side Shield) as a Function of $\theta(\rho = 40$ cm).

on the outside rear of the crew compartment coincident with the reactor tank–detector axis. Check points were taken at least twice, before and after each θ traverse, and these points were maintained to within a maximum of ±6.0% error. With the precautions taken, the statistical error would add ±1% to the error value.

The difference between the curves of air-scattered dose rate measured in air and in the crew compartment with no water side shielding, as shown in Figs. 6.1.4 and 6.1.5, can be attributed largely to the blocking of low-angle air-scattered neutrons by the rear shadow shield, although the attenuation of the aluminum and the different d distances for the two measurements also contribute.

The dose rates measured in the crew compartment with oil used as the side shielding are shown in Figs. 6.1.6 and 6.1.7 and in Table 6.1.3. The curves plotted from the data have approximately the same shapes as the curves in Figs. 6.1.4 and 6.1.5 (for water side shield), but on the average they are slightly lower.

An analysis of the oil used in the experiment showed that it contained nearly the same hydrogen density as water (the measured hydrogen density was 12.7 wt % and the specific gravity was 0.872). Because the hydrogen density was the same in both cases and because the macroscopic removal cross sections for oxygen and carbon are nearly the same, it would not be expected that the attenuations for the two cases would be markedly different. This analysis was confirmed by the measurements, since experimental errors could account for the differences.

Dose-rate measurements were also taken at the center of the crew compartment as the individual 2-in.-thick side tanks were drained from the rear of the crew compartment to the front in successive

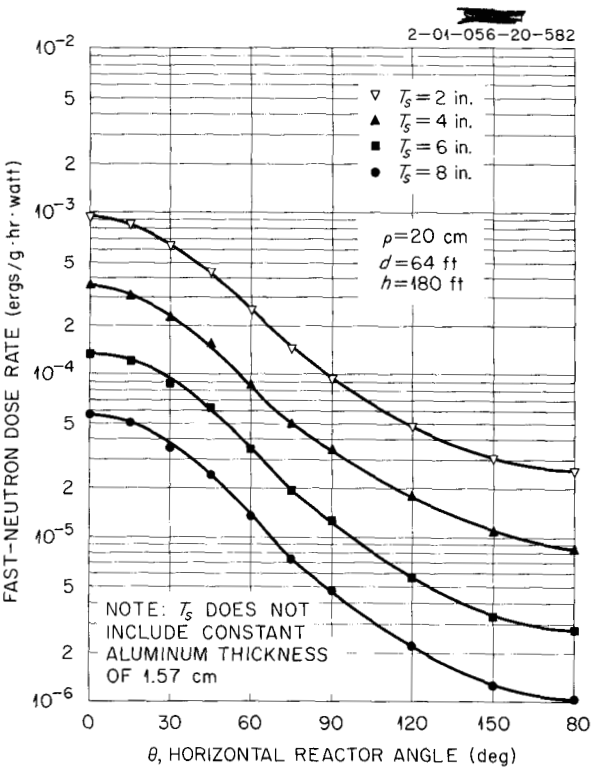

Fig. 6.1.6. Fast-Neutron Dose Rates in the Crew Compartment (Oil Side Shield) as a Function of $\theta(\rho =$ 20 cm).

Table 6.1.2. Fast-Neutron Dose Rates in the Center of the Crew Compartment for Various Water Side Shield Thicknesses

θ (deg)	Fast-Neutron Dose Rate (ergs/g·hr·w)				
	$T_s = 0$	$T_s = 8$ in.	$T_s = 6$ in.	$T_s = 4$ in.	$T_s = 2$ in.
			ρ = 20 cm		
0	2.78×10^{-3}	7.25×10^{-5}	1.66×10^{-4}	4.08×10^{-4}	1.18×10^{-3}
15	2.52×10^{-3}	6.20×10^{-5}	1.47×10^{-4}	3.36×10^{-4}	1.01×10^{-3}
				3.47×10^{-4}	
30	1.78×10^{-3}	4.67×10^{-5}	1.14×10^{-4}	2.65×10^{-4}	7.66×10^{-4}
45	1.23×10^{-3}	3.22×10^{-5}	7.67×10^{-5}	1.83×10^{-4}	5.29×10^{-4}
60	7.03×10^{-4}	1.76×10^{-5}	4.32×10^{-5}	1.07×10^{-4}	2.89×10^{-4}
75	4.24×10^{-4}	9.56×10^{-6}	2.47×10^{-5}	5.61×10^{-5}	1.59×10^{-4}
90	2.85×10^{-4}	6.29×10^{-6}	1.54×10^{-5}	3.73×10^{-5}	1.06×10^{-4}
120	1.58×10^{-4}	2.85×10^{-6}	7.42×10^{-6}	1.86×10^{-5}	5.53×10^{-5}
150	1.11×10^{-4}	1.73×10^{-6}	4.62×10^{-6}	1.20×10^{-5}	3.60×10^{-5}
180	9.53×10^{-5}	1.45×10^{-6}	3.65×10^{-6}	9.55×10^{-6}	3.09×10^{-5}
			ρ = 40 cm		
0	1.60×10^{-4}	6.14×10^{-6}	1.38×10^{-5}	2.94×10^{-5}	7.47×10^{-5}
15	1.41×10^{-4}	5.42×10^{-6}	1.23×10^{-5}	2.57×10^{-5}	6.39×10^{-5}
30	1.01×10^{-4}	3.88×10^{-6}	8.52×10^{-6}	1.84×10^{-5}	4.53×10^{-5}
				1.75×10^{-5}	
45	7.11×10^{-5}	2.59×10^{-6}	5.95×10^{-6}	1.23×10^{-5}	3.12×10^{-5}
60	3.94×10^{-5}	1.42×10^{-6}	3.30×10^{-6}	6.99×10^{-6}	1.76×10^{-5}
75	2.36×10^{-5}	8.11×10^{-7}	1.84×10^{-6}	4.05×10^{-6}	1.00×10^{-5}
90	1.54×10^{-5}	4.93×10^{-7}	1.17×10^{-6}	2.61×10^{-6}	6.37×10^{-6}
120	9.02×10^{-6}	2.26×10^{-7}	5.51×10^{-7}	1.36×10^{-6}	3.44×10^{-6}
150	6.36×10^{-6}	1.36×10^{-7}	3.35×10^{-7}	8.22×10^{-7}	2.5×10^{-6}
180	5.48×10^{-6}	1.03×10^{-7}	2.54×10^{-7}	6.19×10^{-7}	1.95×10^{-6}

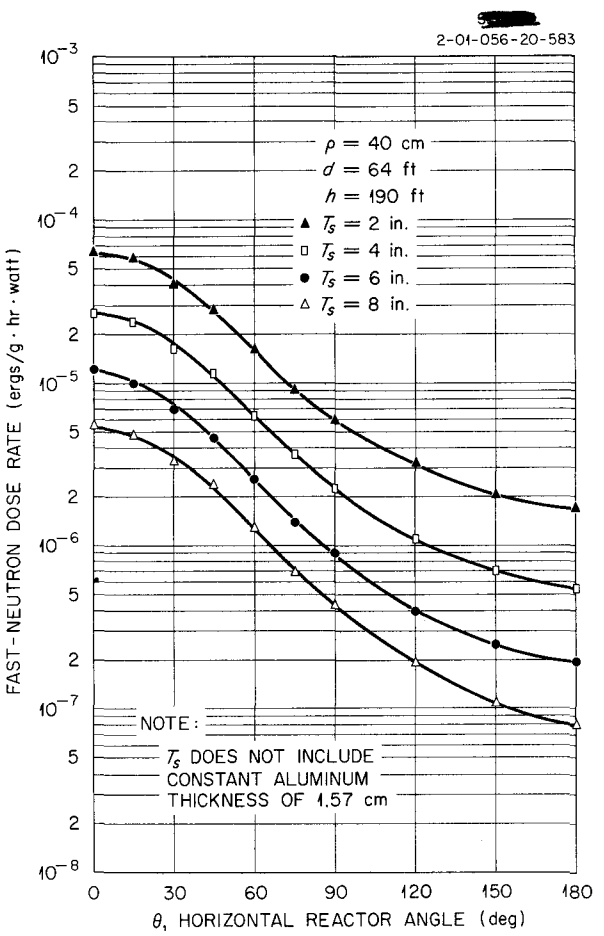

Fig. 6.1.7. Fast-Neutron Dose Rates in the Crew Compartment (Oil Side Shield) as a Function of θ(ρ = 40 cm).

layers. First a measurement was taken with all the tanks filled with water. Then tank No. 15 (see Fig. 6.1.8) was drained and another measurement was made, after which tank No. 20 was drained, etc. This procedure was continued until all the tanks in all four layers had been drained. The results are presented in Fig. 6.1.9 and Table 6.1.4. Since the draining of the layers occurred on different days, there are noticeable differences in some measurements which represent the same shield configurations. These differences are considered to be experimental errors.

From the measurements described above, the relative effectiveness of each individual tank in each layer was determined. In order to do this the dose rate measured immediately preceding the draining of a tank was subtracted from the dose rate measured immediately following the draining of the tank. Similarly, the dose rate measured with all the tanks filled was subtracted from the dose rate measured with all the tanks in the layer drained. The ratio of these two differences represented the percentage dose rate which had arrived through the single tank. Average slant thicknesses were then computed for each tank, based on the average angle η (the angle that the entering radiation was assumed to have made with the reactor tank–detector axis). Weighting factors obtained from a direct-beam attenuation curve, previously reported,[3] were applied to the percentage dose rate for each tank to adjust the value for the difference in attenuation resulting from the slant thickness. The resulting corrected percentage

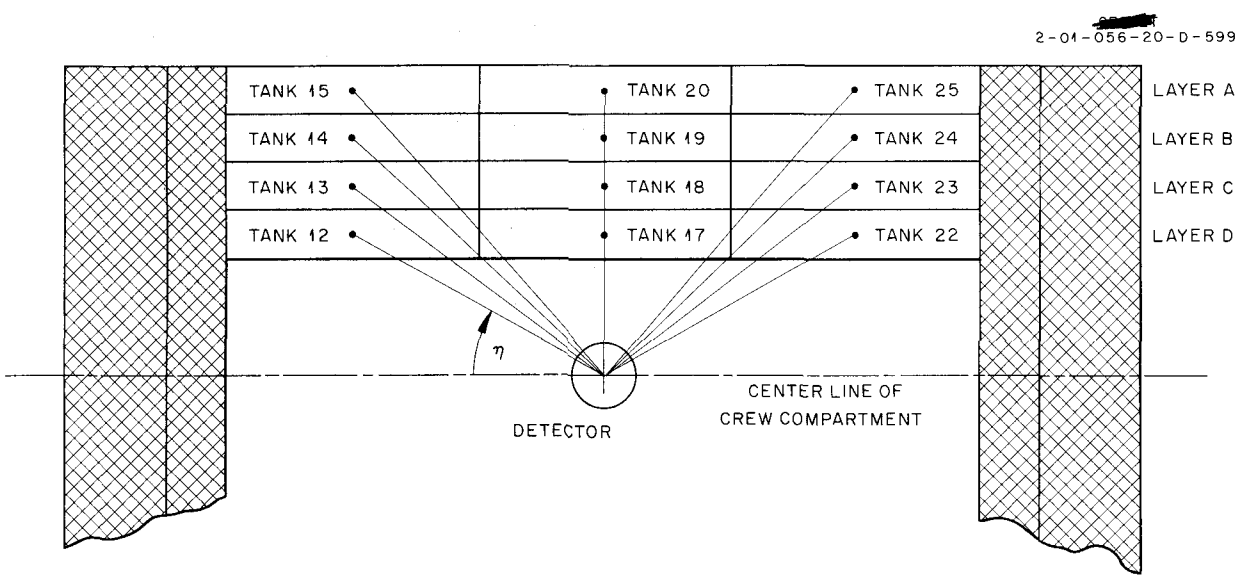

Fig. 6.1.8. Crew-Compartment Geometry for Determining Relative Effectiveness of Individual Shield Tanks.

Table 6.1.3. Fast-Neutron Dose Rates in the Center of the Crew Compartment for Various Oil Side Shield Thicknesses

θ (deg)	Fast-Neutron Dose Rate (ergs/g·hr·w)				
	$T_s = 8$ in.	$T_s = 6$ in.	$T_s = 4$ in.	$T_s = 2$ in.	$T_s = 0$
			$\rho = 20$ cm		
0	5.72×10^{-5}	1.34×10^{-4}	3.58×10^{-4}	9.47×10^{-4}	2.78×10^{-3}
15	5.15×10^{-5}	1.21×10^{-4}	3.09×10^{-4}	8.49×10^{-4}	2.52×10^{-3}
30	3.58×10^{-5}	8.95×10^{-5}	2.26×10^{-4}	6.23×10^{-4}	1.78×10^{-3}
45	2.47×10^{-5}	6.43×10^{-5}	1.58×10^{-4}	4.42×10^{-4}	1.23×10^{-3}
60	1.34×10^{-5}	3.53×10^{-5}	8.85×10^{-5}	2.50×10^{-4}	7.04×10^{-4}
75	7.27×10^{-6}	1.94×10^{-5}	4.96×10^{-5}	1.44×10^{-4}	4.24×10^{-4}
90	4.72×10^{-6}	1.25×10^{-5}	3.45×10^{-5}	9.47×10^{-5}	2.85×10^{-4}
120	2.22×10^{-6}	5.74×10^{-6}	1.77×10^{-5}	4.82×10^{-5}	1.58×10^{-4}
150	1.27×10^{-6}	3.39×10^{-6}	1.06×10^{-5}	2.99×10^{-5}	1.11×10^{-4}
180	1.03×10^{-6}	2.77×10^{-6}	8.45×10^{-6}	2.54×10^{-5}	9.53×10^{-5}
			$\rho = 40$ cm		
0	5.42×10^{-6}	1.23×10^{-5}	2.68×10^{-5}	6.25×10^{-5}	1.60×10^{-4}
15	4.73×10^{-6}	1.01×10^{-5}	2.38×10^{-5}	5.74×10^{-5}	1.41×10^{-4}
30	3.28×10^{-6}	6.92×10^{-6}	1.62×10^{-5}	4.00×10^{-5}	1.01×10^{-4}
45	2.33×10^{-6}	4.70×10^{-6}	1.15×10^{-5}	2.77×10^{-5}	7.11×10^{-5}
60	1.27×10^{-6}	2.58×10^{-6}	6.48×10^{-6}	1.60×10^{-5}	3.94×10^{-5}
75	6.78×10^{-7}	1.38×10^{-6}	3.63×10^{-6}	8.94×10^{-6}	2.36×10^{-5}
90	4.28×10^{-7}	9.11×10^{-7}	2.27×10^{-6}	5.84×10^{-6}	1.54×10^{-5}
120	1.93×10^{-7}	3.98×10^{-7}	1.11×10^{-6}	3.25×10^{-6}	9.02×10^{-6}
150	1.08×10^{-7}	2.49×10^{-7}	7.08×10^{-7}	2.06×10^{-6}	6.36×10^{-6}
180	7.96×10^{-8}	1.94×10^{-7}	5.50×10^{-7}	1.71×10^{-6}	5.48×10^{-6}

dose rate for each individual tank was divided by the total solid angle subtended by the tank at the detector in order to determine the average percentage dose rate per unit solid angle. The results are shown in Fig. 6.1.10, in which the points are plotted as a function of the average angle η at the detector.

Determination of the Air-Scattering Probabilities

The probability of air-scattered fast neutrons penetrating to the center of a cylindrical crew compartment is defined as the measured air-scattered dose rate reaching the center of the crew shield divided by the total direct-beam dose rate leaving the reactor, as given below:

$$P^{s}_{s,c}(\theta, T_s) = \frac{D^{s}_{s,c}(\theta, T_s)}{2\pi l^2 \int_0^{\pi} D_d(\theta) \sin\theta \, d\theta} ,$$

Table 6.1.4. Fast-Neutron Dose Rates at the Center of the Crew Compartment for Various Water Side Shield Configurations

$\theta = 0$ deg, $d = 64$ ft, $h = 190$ ft, $\rho = 20$ cm

Tank Configuration	Fast-Neutron Dose Rate* (ergs/g·hr·w)			D_t/D_L Measured	D_t/D_L Corrected	Average Percentage Dose Rate Per Unit Solid Angle
	D_T	D_t	D_L			
$T_s = 8$ in.	7.07×10^{-5}					
Drain 15	9.22×10^{-5}	2.15×10^{-5}		0.249	0.366	14.9
Drain 20	1.42×10^{-4}	4.98×10^{-5}		0.579	0.378	6.9
Drain 25	1.57×10^{-4}	1.50×10^{-5}	8.6×10^{-5}	0.174	0.256	10.45
$T_s = 6$ in.	1.57×10^{-4}					
Drain 14	2.19×10^{-4}	6.2×10^{-5}		0.284	0.393	16.4
Drain 19	3.40×10^{-4}	1.21×10^{-5}		0.555	0.384	6.54
Drain 24	3.75×10^{-4}	3.5×10^{-5}	2.18×10^{-4}	0.161	0.223	9.37
$T_s = 4$ in.	4.08×10^{-4}**					
Drain 13	6.19×10^{-4}	2.11×10^{-4}		0.323	0.410	17.7
Drain 18	9.7×10^{-4}	3.51×10^{-4}		0.538	0.415	6.56
Drain 23	1.06×10^{-3}	9.0×10^{-5}	6.52×10^{-4}	0.138	0.175	7.68
$T_s = 2$ in.	1.15×10^{-3}**					
Drain 12	1.89×10^{-3}	7.4×10^{-4}		0.389	0.442	20.7
Drain 17	2.78×10^{-3}	8.9×10^{-4}		0.468	0.397	5.79
Drain 22	3.05×10^{-3}	2.7×10^{-4}	1.90×10^{-3}	0.142	0.161	7.39

*D_T = total dose rate measured at center of crew compartment;

D_t = total dose rate which arrived through the last tank drained, i.e., the difference between two consecutive values of D_T;

D_L = total dose rate which arrived through the last three-tank layer drained.

**The difference between this value and the preceding entry in this column is attributed to the measurements having been made on different days.

or, as is usually written,

$$l^2 P^s_{s,c}(\theta, T_s) = \frac{D^s_{s,c}(\theta, T_s)}{2\pi \int_0^\pi D_d(\theta) \sin\theta \, d\theta},$$

where

$D^s_{s,c}(\theta, T_s)$ = air-scattered dose rate, measured at the center of the crew compartment, which arrives through the side of the crew compartment T_s thick as a function of the beam angle θ,

l = separation distance between the center of the reactor tank and the detector,[5]

$D_d(\theta)$ = direct-beam dose rate measured at the distance l as a function of the beam angle θ.

[5]It should be pointed out that l for the in-air measurements is equivalent to d for the in-air measurements (that is, $l = d = 61.5$ ft), whereas l for the crew-compartment measurements is equivalent to d plus the 4.2 ft from the rear of the crew compartment to its center (that is, $l = 64 + 4.2$ ft). However, the final probabilities obtained in the calculation are for $l = 64$ ft.

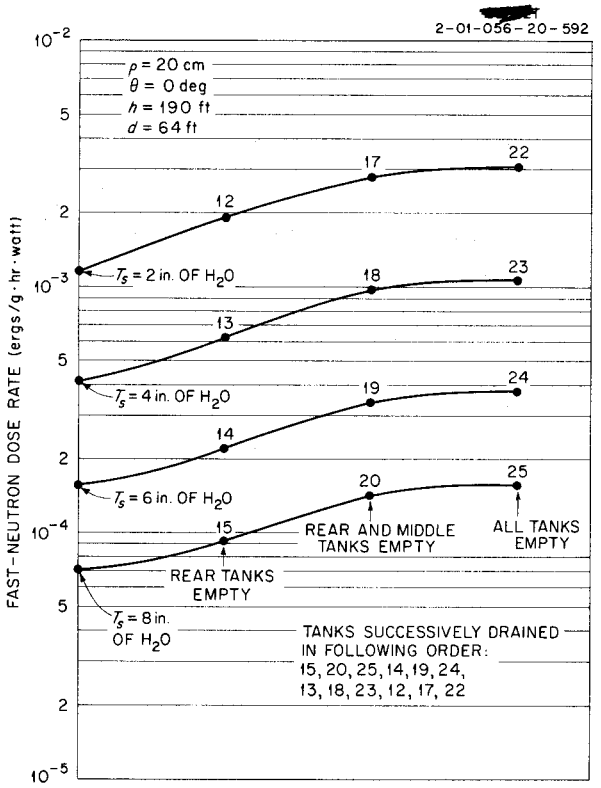

Fig. 6.1.9. Fast-Neutron Dose Rates in the Crew Compartment for Various Water Side Shield Configurations.

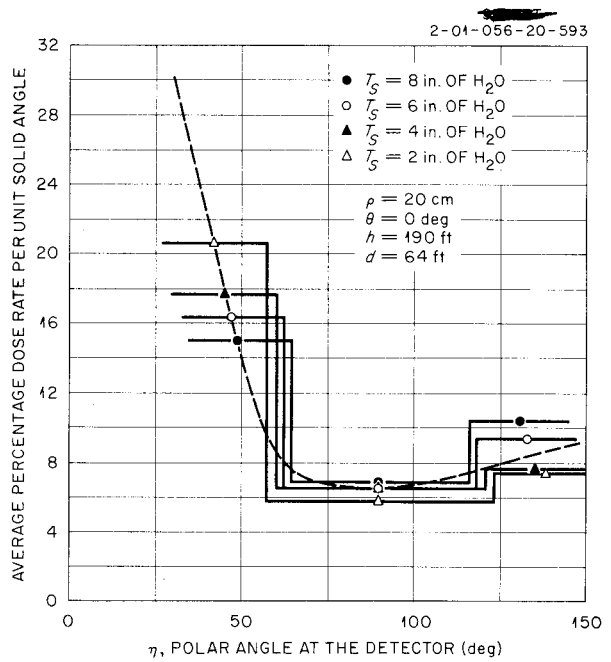

Fig. 6.1.10. Average Percentage Dose Rate Entering the Side of the Crew Compartment as a Function of η for Various Side Shield Thicknesses.

If it is desired to calculate the air-scattered dose rate from an isotropic source with a shield of irregular shape (Fig. 6.1.11*a*) which penetrates the sides of a cylindrical crew shield, the expression used, in general, is

$$D^s_{s,c} = \int_A D_d(a,l)\, e^{-\int_0^{T_d} dt/\lambda_d} [l^2 P^s_{s,c}(\theta, T_s)]\, dA \ ,$$

where

a = radius of a spherical shield at the source,

T_d = variable thickness of a shield of irregular shape outside the spherical shield at the source,

λ_d = relaxation length of the direct beam in the shield at the source,

$D_d(a, l)$ = direct-beam dose rate at a distance l from dose rate leaving the spherical shield.

The integration is performed over the surface (A) of the reactor shield.

For a conical-shell reactor shield, such as that shown in Fig. 6.1.11*b*, which is the configuration that was previously used for the optimization of a neutron reactor shield,[6] the expression for the total air-scattered dose rate at the center of the crew compartment becomes

$$D^s_{s,c} = \sum_{n=1}^{N} D^s_{s,c,n} = \sum_{n=1}^{N} \int_{\cos\theta_n'}^{\cos\theta_n''} \int_{\psi=0}^{2\pi} D_d(a,l)\, e^{-\int_0^{T_n} dt/\lambda_d} [l^2 P^s_{s,c}(\theta_n, T_s)]\, d\theta\, d(\cos\theta) \ ,$$

[6] M. F. Valerino and F. L. Keller, *ANP Quar. Prog. Rep. Sept. 10, 1955*, ORNL-1947, p 205.

UNCLASSIFIED
2-01-056-20-D-600

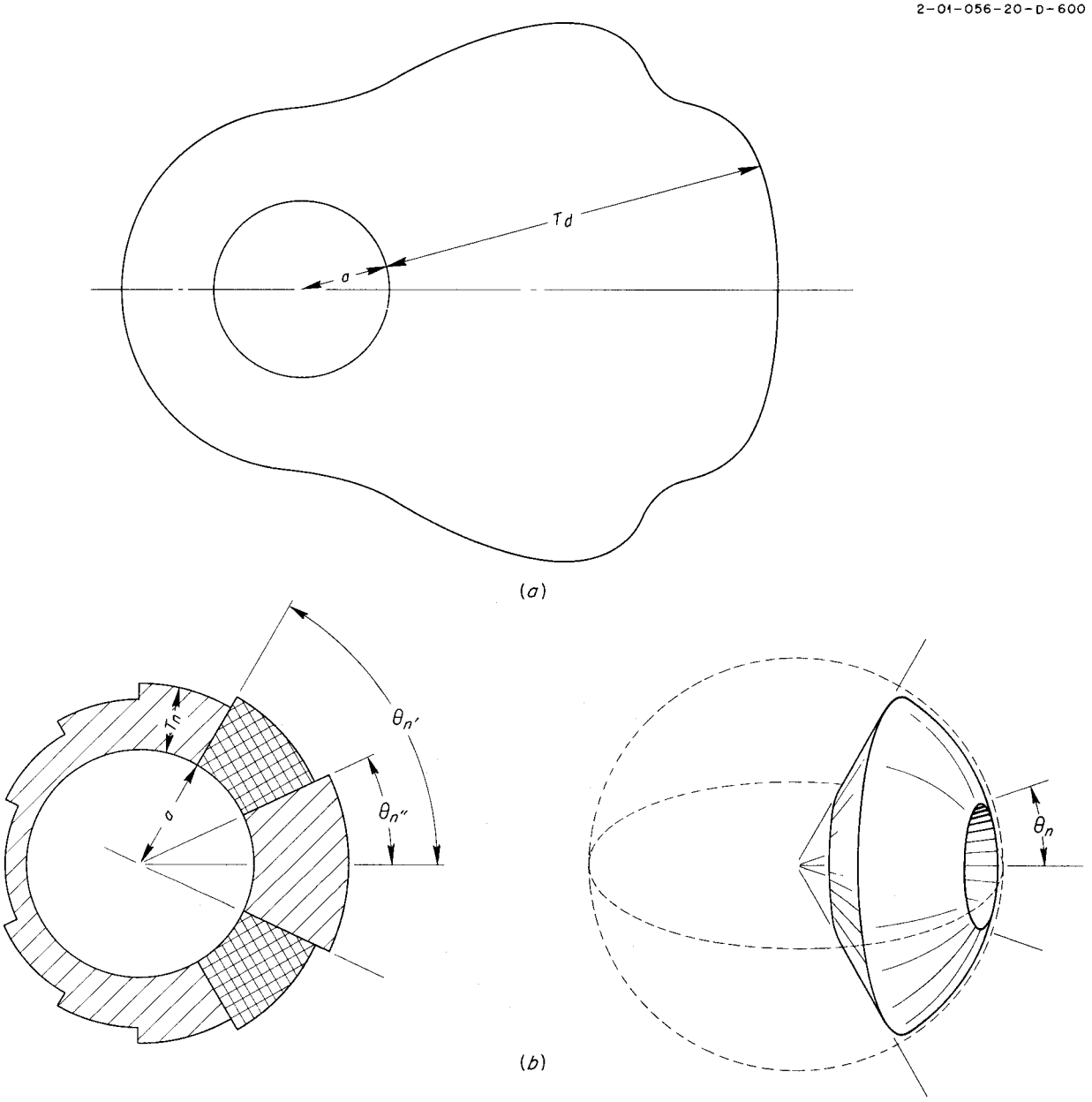

Fig. 6.1.11. Geometry Used To Determine Air-Scattering Probabilities.

where

$D^{s}_{s,c,n}$ = air-scattered dose rate at the center of the crew compartment resulting from the dose rate leaving the nth conical shell at the reactor,

θ_n'', θ_n' = boundary angles of the nth conical shell,

N = total number of conical shells,

ψ = azimuthal angle,

T_n = shield thickness for the nth conical shell,

$P^{s}_{s,c}(\theta_n, T_s)$ = average value of the air-scattering probability for the nth shell.

Upon integrating, the expression becomes

$$D^s_{s,c} = \sum_{n=1}^{N} (\cos\theta_n'' - \cos\theta_n') \left[D_d(a,l)\, e^{-\int_0^{T_n} dt/\lambda_d} \right] \left[2\pi l^2 P^s_{s,c}(\theta_n, T_s) \right]$$

or

$$D^s_{s,c} = \sum_{n=1}^{N} (\cos\theta_n'' - \cos\theta_n')\, D_d(a,l)\, e^{-\int_0^{T_n} dt/\lambda_d} \left[2\pi l^2 P^s_{s,c}(\theta_n, T_s = 0) \right] e^{-\int_0^{T_s} dt/\lambda^s_s} ,$$

where λ^s_s is the relaxation length of the dose rate in the side of the crew compartment.

Since in all previous experiments at the TSF the thickness of the shield on the side of the crew compartment could not be varied, no measurements could be made at the center of the cavity as a function of the side shield thickness. Therefore the probabilities previously calculated were based on measurements made at various distances inside the detector tank and represented the probability, $l^2P^s(\theta)$, of air-scattered neutrons reaching the surface of a cylindrical crew compartment. To calculate the dose rate which would result at the center of the cavity it was necessary not only to multiply this probability by an attenuation term,

$$e^{-\int_0^{T_s} dt/\lambda^s_s} ,$$

but also by a focusing factor, f^s_s, to account for the focusing of the radiation at the center of the crew compartment. Since in the present experiment it was possible to make measurements at the center of the cavity as a function of T_s, the new probability term, $2\pi l^2 P^s_{s,c}(\theta, T_s)$, is equivalent to the product of the terms

$$l^2P^s(\theta),\ f^s_s,\ \text{and}\ e^{-\int_0^{T_s} dt/\lambda^s_s} ;$$

therefore, the necessity of using the focusing factor, for which reliable values are as yet unobtainable (see below), is eliminated. (The 2π in the new probability term is required because the definition of the old probability term included the integral of $d\phi$ over 2π radians.)

The probabilities of the air-scattered neutrons reaching the center of the crew compartment as determined from the new measurements are plotted as a function of θ in Figs. 6.1.12 and 6.1.13 for $\rho = 20$ and 40 cm, respectively. The same values are plotted as a function of the water side shield thickness at the crew compartment in Figs. 6.1.14 and 6.1.15.

[redacted]

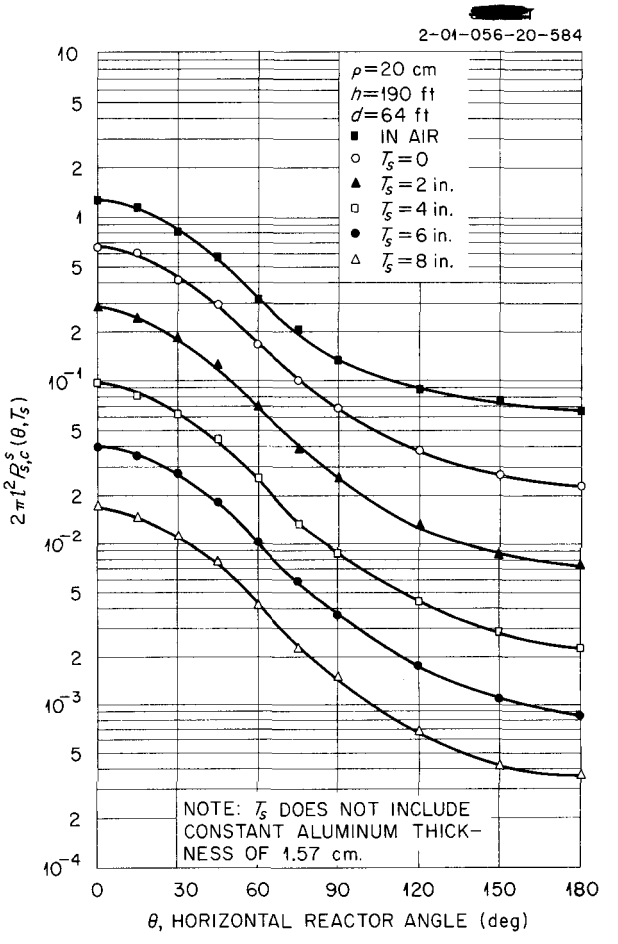

Fig. 6.1.12. Probability of Fast Neutrons from a Conical-Shell Beam Scattering to the Center of the Crew Compartment as a Function of θ for $\rho = 20$ cm.

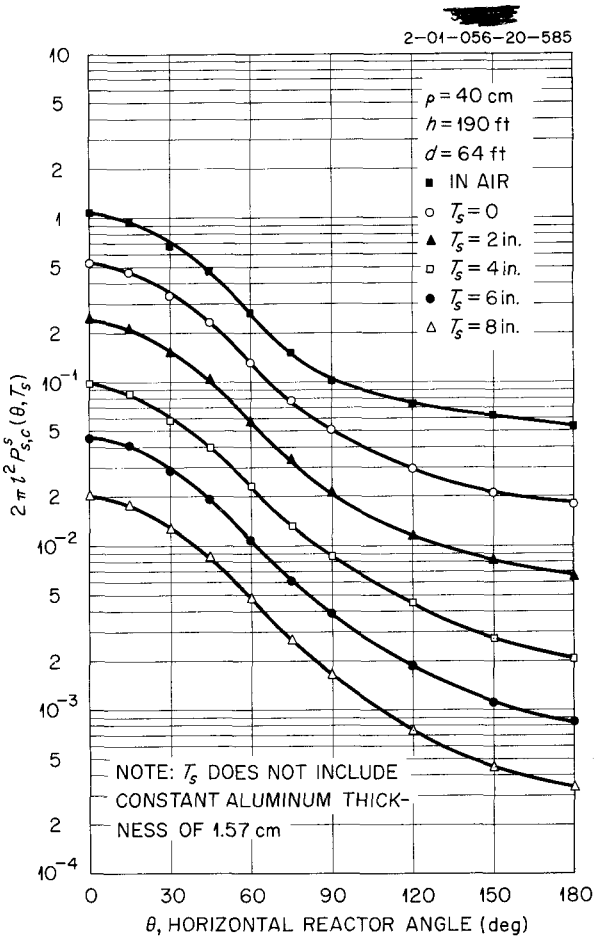

Fig. 6.1.13. Probability of Fast Neutrons from a Conical-Shell Beam Scattering to the Center of the Crew Compartment as a Function of θ for $\rho = 40$ cm.

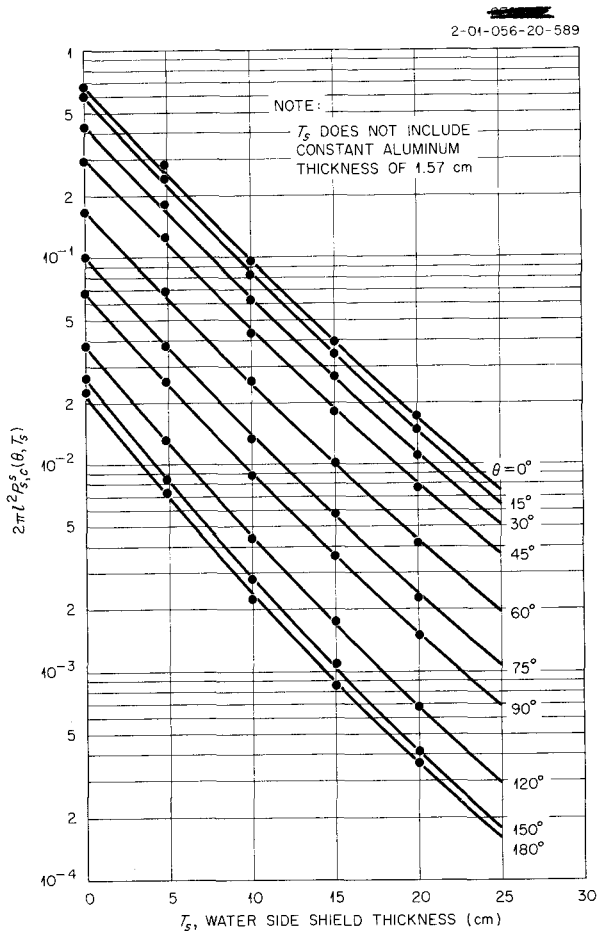

Fig. 6.1.14. Probability of Fast Neutrons from a Conical-Shell Beam Scattering to the Center of the Crew Compartment as a Function of T_s for $\rho = 20$ cm.

The focusing factor used with the previous method was calculated on the basis of measurements made in a cylindrical crew compartment with a constant side shield thickness of 37 cm.[7] The value for this thickness did not appear to be dependent on θ, so an average value of 5.12 was used. Since measurements could be made in the present experiment not only as a function of θ but also as a function of T_s and since

$$f_s^s(\theta, T_s) = \frac{2\pi l^2 P^s_{s,c}(\theta, T_s)}{l^2 P^s(\theta)\, e^{-\int_0^{T_s} dt/\lambda_s^s}},$$

values of f_s^s could be computed for other side shield thicknesses. The results are presented in Fig. 6.1.16 and Table 6.1.5. (The plotted values for the various thicknesses represent average values for ρ = 20 and 40 cm, since, within the experimental error, the scattering probabilities are independent of ρ for the two values taken.) With the exception of the θ = 180-deg points, the values of f_s^s for the four thicknesses at any value of θ fall within the limits of experimental error. Therefore, the curve of average value of the plotted points is shown. This average curve, as drawn,

[7] J. E. Van Hoomissen, *ANP Quar. Prog. Rep. June 10, 1955*, ORNL-1896, p 217, esp Table 14.1.

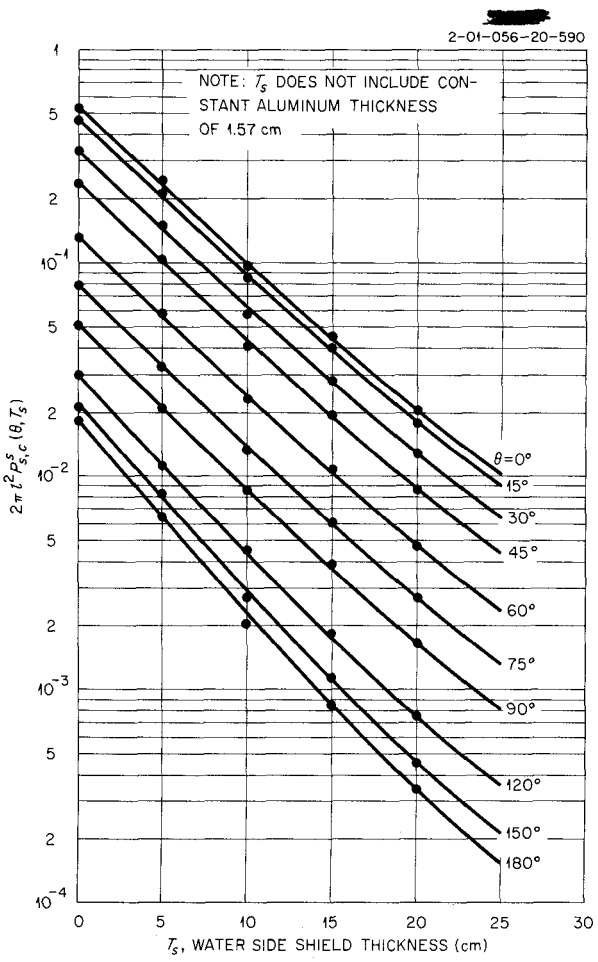

Fig. 6.1.15. Probability of Fast Neutrons from a Conical-Shell Beam Scattering to the Center of the Crew Compartment as a Function of T_s for $\rho = 40$ cm.

shows that f^s_s is dependent on θ in the region between $\theta = 0$ and $\theta = 90$ deg.

Relaxation Lengths in the Water in the Crew-Compartment Side Shield

Incremental relaxation lengths for the fast neutrons penetrating the sides of a cylindrical crew compartment and reaching the center, as a function of the horizontal reactor angle θ and the side shielding thickness T_s, are parameters needed in the method presently used for optimum neutron shield design.

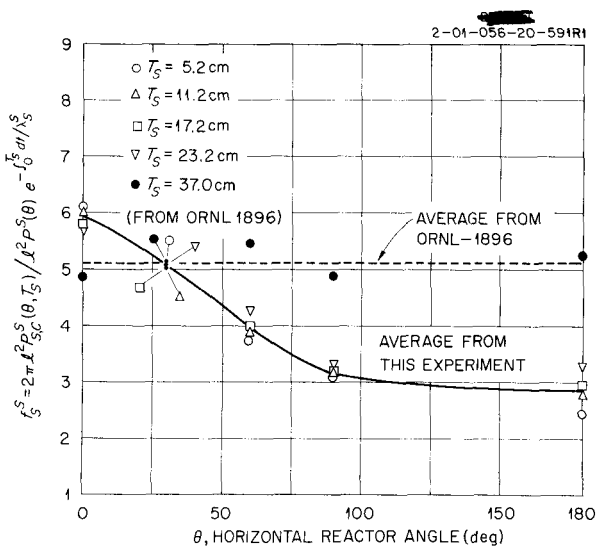

Fig. 6.1.16. Focusing Factor, f^s_s, for Fast Neutrons from a Conical-Shell Beam Entering the Sides of the Crew Compartment.

Table 6.1.5. Average Values of f^s_s for Various Values of θ and T_s

T_s(cm)	f^s_s				
	$\theta = 0$ deg	$\theta = 30$ deg	$\theta = 60$ deg	$\theta = 90$ deg	$\theta = 180$ deg
5.2	6.12	5.19	3.75	3.09	2.43
11.2	6.02	5.04	3.89	3.14	2.77
17.2	5.81	5.03	4.01	3.20	2.94
23.2	5.72	5.09	4.30	3.33	3.29
Av	5.91	5.09	3.99	3.18	2.85

The instantaneous relaxation lengths, λ_i, for each 2-in. increment, Δt, of side shielding in the crew compartment were calculated from the basic attenuation equation

$$D_1 = D_2 e^{-t/\lambda_i} ,$$

where D_1 and D_2 are the experimentally measured dose rates before and after the addition of each 2-in. increment of side shield. Because of the size of the increments, the differences in the measured dose rates were relatively small, and thus the values of fhe exponential and consequently the values of the incremental relaxation lengths are subject to appreciable error. In order to minimize the error, the data used in the calculations were appropriately smoothed. The method of calculation entailed normalizing the fast-neutron dose rate vs θ curves to one point (θ = 0 deg) and adjusting the curves, based on experience, to present a consistent pattern.

The adjusted curves were then cross plotted as a function of the actual crew-compartment side shield thickness to obtain the attenuation curves. The best smooth curves were drawn through the plotted points, and dose-rate values taken from the curves were used to calculate the instantaneous relaxation lengths. The results are shown in Figs. 6.1.17 and 6.1.18 as a function of the horizontal reactor angle θ for ρ = 20 and 40 cm, respectively.

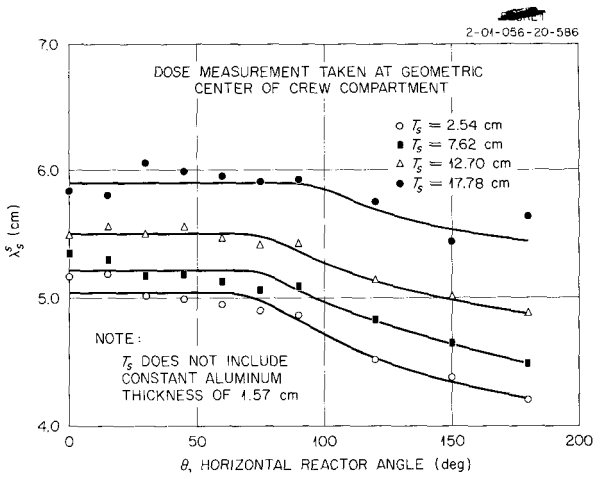

Fig. 6.1.17. Instantaneous Relaxation Lengths for Fast Neutrons Scattered from a Conical-Shell Beam Through the Crew-Compartment Water Side Shield as a Function of θ for ρ = 20 cm.

Relaxation lengths for ρ = 40 cm were also calculated from the values found at ρ = 20 cm by making use of the relation[5]

$$\lambda_s^s(40, T_s) = \frac{\lambda_s^s(20, T_s)}{\lambda_d(20 + T_s)} \lambda_d(40 + T_s) .$$

The results, shown in Table 6.1.6, agree with the measured values to within a 7% error.

This relation was also used to calculate relaxation lengths for the ρ = 45 cm case by using both ρ = 20 and 40 cm data. Averages of the results were taken for comparison with relaxation lengths measured with the detector tank,[5] and the comparison is presented in graphical form in Fig. 6.1.19. The values obtained from this experiment are approximately 15% higher than those calculated from the detector tank data, but they are considered to be more accurate, since they were obtained directly from two measured dose-rate values which included the effect of the focusing in the cavity of the crew compartment. The earlier calculations from detector tank data involved an integration with respect to the azimuthal angle for each point on the attenuation curve, and therefore they were susceptible to greater error.

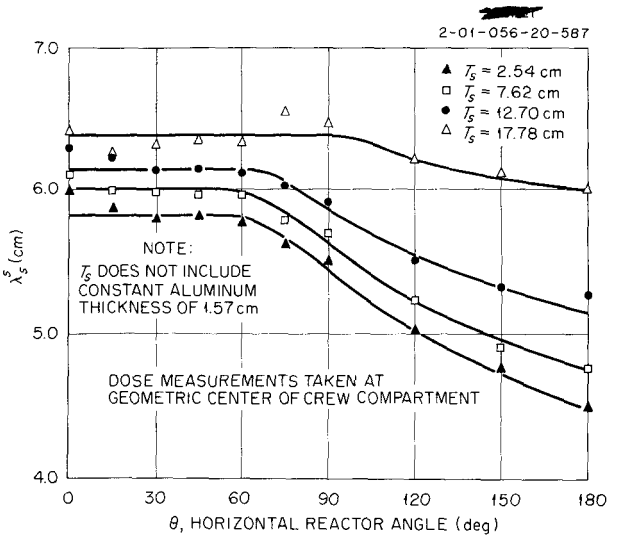

Fig. 6.1.18. Instantaneous Relaxation Lengths for Fast Neutrons Scattered from a Conical-Shell Beam Through the Crew-Compartment Water Side Shield as a Function of θ for ρ = 40 cm.

Table 6.1.6. Comparison of Measured and Calculated* Values of λ_s^s for $\rho = 40$ cm

θ (deg)	$\lambda_s^s(40, T_s)$ (cm)							
	$T_s = 5.08$ cm		$T_s = 10.16$ cm		$T_s = 15.24$ cm		$T_s = 20.32$ cm	
	Measured	Calculated	Measured	Calculated	Measured	Calculated	Measured	Calculated
0	5.82	5.80	6.0	5.90	6.14	6.22	6.38	6.55
15	5.82	5.80	6.0	5.90	6.14	6.22	6.38	6.55
30	5.82	5.80	6.0	5.90	6.14	6.22	6.38	6.55
45	5.82	5.80	6.0	5.90	6.14	6.22	6.38	6.55
60	5.81	5.80	5.98	5.90	6.14	6.22	6.38	6.55
75	5.66	5.73	5.84	5.88	6.06	6.20	6.38	6.55
90	5.43	5.55	5.61	5.71	5.86	6.07	6.38	6.53
120	5.03	5.20	5.24	5.45	5.55	5.79	6.21	6.32
150	4.73	5.00	4.96	5.24	5.33	5.64	6.08	6.15
180	4.51	4.84	4.77	5.07	5.16	5.51	6.00	6.04

*From the equation: $\lambda_s^s(40, T_s)(\text{Calculated}) = \lambda_s^s(20, T_s)(\text{Measured}) \dfrac{\lambda_d(40 + T_s)(\text{Measured})}{\lambda_d(20 + T_s)(\text{Measured})}$, where λ_d is the fast-neutron relaxation length in the reactor wall shield.

[redacted]

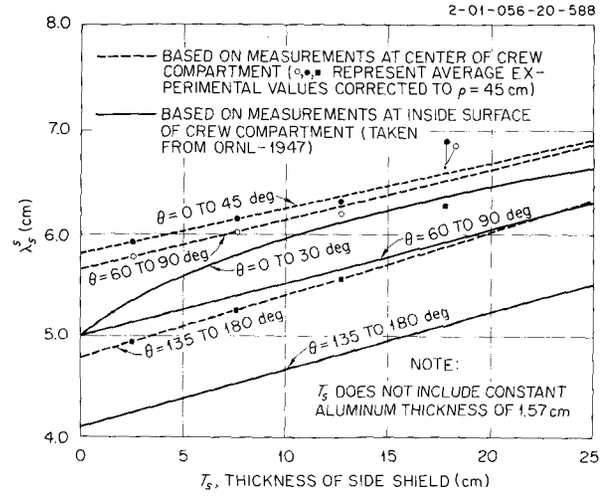

Fig. 6.1.19. Instantaneous Relaxation Lengths for Fast Neutrons Scattered from a Conical-Shell Beam Through the Crew-Compartment Water Side Shield as a Function of the Thickness of the Side Shield.